Spike-Type Solutions to One Dimensional Gierer–Meinhardt Model with Lévy Flights

By Y. Nec

The Gierer–Meinhardt model with Lévy flights is shown to give rise to patterns of spikes with algebraically decaying tails. The spike shape is given by a solution to a fractional differential equation. Near an equilibrium formation the spikes drift according to the differential equations of the form known for Fickian diffusion, but with a new homoclinic. A nonlocal eigenvalue problem of a new type is formulated and studied. The system is less stable due to the Lévy flights, though the behavior of eigenvalues is changed mainly quantitatively.

1. Introduction

This paper is concerned with the analysis of motion and stability of spike-type solutions for a two component reaction—diffusion system allowing for a diffusion anomaly of the type Lévy flights. A short overview of Lévy flights and related fractional operators is given before the description of the model.

1.1. Lévy flights

In the formalism of the continuous time random walk a particle location evolves according the probability to make a step of length $\mathfrak{r}$ after time t

$$\psi(\mathfrak{r}, t) = w(t)\,\mathfrak{m}(\mathfrak{r}),$$

where $w(t)$ and $\mathfrak{m}(\mathfrak{r})$ are waiting time and step length probability density functions, respectively. Regular Fickian diffusion, i.e. $\langle \mathfrak{r}^2(t)\rangle \sim t$, ensues when

Address for correspondence: Yana Nec, Department of Mathematics, University of British Columbia, 1984 Mathematics Road, Vancouver, V6T1Z2, BC, Canada; e-mail: oulanka@math.ubc.ca

DOI: 10.1111/j.1467-9590.2012.00550.x
STUDIES IN APPLIED MATHEMATICS 129:272–299

$\mathfrak{m}(\mathfrak{r})$ is Gaussian and $w(t) = \frac{1}{\tau_*} e^{-t/\tau_*}$, with $0 < \tau_* \sim \mathcal{O}(1)$ being a characteristic time scale. Lévy flight is a diffusion anomaly, where the step length probability density function possesses an algebraic decay

$$\mathfrak{m}(\mathfrak{r}) \sim \frac{1}{\mathfrak{r}^{\gamma+1}}, \quad \mathfrak{r} \gg 1, \quad 1 \leq \gamma < 2,$$

rendering the second moment $\langle \mathfrak{r}^2(t) \rangle$ divergent for any finite t. The continuum limit operator $\partial_t - \Delta$ in the diffusion equation is then replaced by a fractional operator [1] $\partial_t + (-\Delta)^{\gamma/2}$.

Observations of super-diffusion of the type Lévy flights in nature have been reported and analyzed in the past two decades in quite a few unrelated fields. Some examples are fluid dynamics [2, 3], polymers [4], granular materials [5] and animal motion [6]. As the measurement techniques advance, the exponent γ is estimated in a growing number of systems, demonstrating that the regular diffusion is only a special limit of a whole family of processes.

1.2. Fractional derivative operators

The fractional derivative is a generalization of the usual integer derivative to an arbitrary order, most generally defined as [7]

DEFINITION 1.

$$ {}_a\mathfrak{D}_x^{\gamma} f(x) = \frac{1}{\Gamma(n-\gamma)} \frac{d^n}{dx^n} \int_a^x \frac{f(\xi)\, d\xi}{(x-\xi)^{\gamma-n+1}}, \quad n-1 \leq \gamma < n, $$
$$ n \in \mathbb{N}, \quad a \in \mathbb{R}. $$

This derivative is clearly asymmetric under the reflexion $x \longmapsto (-x)$. The range of γ relevant to Lévy flights is $1 \leq \gamma < 2$. Using equally weighted combination of the left-hand and right-hand fractional derivatives gives a symmetric operator alias fractional Laplacian in one spatial dimension

DEFINITION 2.

$$ \mathfrak{D}_{|x|}^{\gamma} f(x) = -\frac{\sec \widetilde{\gamma}}{2\Gamma(2-\gamma)} \frac{d^2}{dx^2} \left\{ \int_{-\infty}^x \frac{f(\xi)\, d\xi}{(x-\xi)^{\gamma-1}} + \int_x^{\infty} \frac{f(\xi)\, d\xi}{(\xi-x)^{\gamma-1}} \right\} $$
$$ = \frac{\sec \widetilde{\gamma}}{2\Gamma(-\gamma)} \int_{-\infty}^{\infty} \frac{f(x) - f(\xi)}{|x-\xi|^{\gamma+1}}\, d\xi, \quad \widetilde{\gamma} = \frac{\pi\gamma}{2}, \quad 1 \leq \gamma < 2. $$

Both equalities in Definition 2 are used throughout the paper at convenience for all theoretical derivations. Note that the prefactor is finite at the limit $\gamma \longrightarrow 1$. Definition 2 is generalized to higher dimensions as

DEFINITION 3.

$$-(-\Delta)^{\gamma/2} f(\mathbf{x}) = C_{d,\gamma} \int_{\mathbb{R}^d} \frac{f(\boldsymbol{\xi}) - f(\mathbf{x})}{|\mathbf{x} - \boldsymbol{\xi}|^{d+\gamma}} \, d\boldsymbol{\xi}, \quad C_{d,\gamma} = 2^{\gamma} \frac{\Gamma((d+\gamma)/2)}{\pi^{d/2} |\Gamma(-\gamma/2)|}, \quad 1 \leq \gamma < 2.$$

For functions on $\mathbb{R}^d$, whose Fourier transform exists, an equivalent definition in Fourier space is

DEFINITION 4.

$$\mathcal{F}_{x \longmapsto q}\{-(-\Delta)^{\gamma/2} f(\mathbf{x})\} = -|\mathbf{q}|^{\gamma} \mathcal{F}_{x \longmapsto q}\{f(\mathbf{x})\}, \quad 1 \leq \gamma \leq 2.$$

This definition is used for the numerical computation of the homoclinic in §3.1. Definition 3 and Definition 2 have improper limits at $\gamma = 2$, whereas Definition 4 is proper at that limit.

1.3. Mathematical model

Fractional diffusion equations [1] have been used to model anomalously slow or fast scattering of particles in a variety of natural applications. The methods of solution of such equations often use integral transforms and special functions for the representation of fundamental solutions [8]. When the diffusion process is accompanied by a nonlinear reaction term, even fewer exact solutions are known than in the case of regular diffusion. One of the better studied types of reaction kinetics is that yielding front solutions [9], and in that case exact solutions for any $1 \leq \gamma \leq 2$ are available only with piecewise linear kinetics [10]. Existence and uniqueness of solutions for a type of nonlinearity yielding homoclinics were studied [11], and an exact solution was given for $\gamma = 1$ (limiting value corresponding to the most extreme Lévy flight).

To the authors' knowledge no stability theories exist for any homoclinic pulse solutions of reaction—diffusion models with super-diffusion. The purpose of the current work is to set a stability theory for a quasi-equilibrium spike pattern subject to Lévy flights.

Spike patterns are functions, whose value is close to a background state in most of the domain of their definition, except for a few localized foci. This behavior is observed, for example, in neural pulses traveling along axons, stripe patterns in the morphogenesis of certain animal species as well as chemical systems. A paradigm for the generation of spike-type solutions is the activator-inhibitor system with Gierer–Meinhardt kinetics (written in dimensionless form)

$$\partial_t a = \epsilon^2 a_{xx} - a + \frac{a^p}{h^q}, \quad -1 < x < 1, \quad t > 0, \tag{1a}$$

$$\tau_o\,\partial_t h = D\,h_{xx} - \mu h + \epsilon^{-1}\frac{a^m}{h^s}, \quad -1 < x < 1, \quad t > 0, \tag{1b}$$

$$a_x(\pm 1, t) = h_x(\pm 1, t) = 0, \quad a(x, 0) = a_0(x), \quad h(x, 0) = h_0(x), \tag{1c}$$

with $a(x, t)$, $h(x, t)$ denoting the activator and inhibitor respective concentrations. In addition, ϵ and D denote the diffusivities, μ is the inhibitor decay rate and τ_o – the reaction time constant. The usual assumption on the exponents (p, q, m, s) is

$$p > 1, \quad q > 0, \quad r > 0, \quad s \geq 0, \quad 0 < \frac{p-1}{q} < \frac{m}{s+1}.$$

A quasi-equilibrium spike solution exists when $0 < \epsilon \ll 1$ and $0 < D \sim \mathcal{O}(1)$. Symmetric and asymmetric combinations of spikes are possible. Stability of symmetric profiles was analyzed separately for the case[12] $\partial_t h \equiv 0$ (or equivalently $\tau_o = 0$) and the generic case [13] $\tau_o > 0$. Asymmetric spike patterns were also investigated [14], but are beyond the scope of this paper.

To incorporate Lévy flights system (1) is modified as

$$\partial_t a = \epsilon^\gamma \mathfrak{D}^\gamma_{|x|} a - a + \frac{a^p}{h^q}, \quad -1 < x < 1, \quad t > 0, \tag{2a}$$

$$\tau_o\,\partial_t h = D\,h_{xx} - \mu h + \epsilon^{-1}\frac{a^m}{h^s}, \quad -1 < x < 1, \quad t > 0, \tag{2b}$$

$$a_x(\pm 1, t) = h_x(\pm 1, t) = 0, \quad a(x, 0) = a_0(x), \quad h(x, 0) = h_0(x), \tag{2c}$$

$$a(x, t) = a(x + 2k, t), \quad h(x, t) = h(x + 2k, t), \quad x \in \mathbb{R},\ t > 0,\ k \in \mathbb{Z}. \tag{2d}$$

The γ-dependent powers of ϵ in system (2) are essential for the existence of a spike pattern. The operator $\mathfrak{D}^\gamma_{|x|}$ requires the values of $a(x, t)$ over $\mathbb{R}$, and thus condition (2d) defines both $a(x, t)$ and $h(x, t)$ on $\mathbb{R}$ by a periodic replication of the pattern. This is possible due to the identical background state of all spikes and Neumann boundary conditions in (2c) that ensure the smoothness of both functions at the juncture points $x = 1 + 2k$. The substitution of $\gamma = 2$ recovers the normal model (1) and condition (2d) is then superfluous.

Model (2) is particularly interesting because of two features. First, the ratio of diffusivities is of order $\mathcal{O}(\epsilon^\gamma)$, i.e. asymptotically larger than $\mathcal{O}(\epsilon^2)$, the ratio required to sustain patterns with regular diffusion. This property is of importance because in actual biological systems it is difficult to justify a ratio of diffusion coefficients as small as $\mathcal{O}(\epsilon^2)$ for two species diffusing in the same medium. A model with a similar feature has recently been studied with sub-diffusion [15], and in this sense the regular diffusion gives the least biologically realistic ratio of activator to inhibitor diffusivities. Second, the super-diffusive species is the usually slow activator, thus creating a tighter

competition between the species. In fact, the effective ratio of the mean square displacement

$$\frac{\langle \mathfrak{r}_{\text{act}}^2(t)\rangle}{\langle \mathfrak{r}_{\text{inh}}^2(t)\rangle} = \frac{\epsilon^\gamma}{D\,t}\int_{-\infty}^{\infty} \mathfrak{r}^2\psi(\mathfrak{r},t)\,d\mathfrak{r}$$

is in favor of the activator (and infinite because the second moment of $\psi(\mathfrak{r},t)$ does not exist) if ϵ is taken finite. At the limit $\epsilon \longrightarrow 0$ the effective ratio is undefined, but the analysis below shows that patterns exist and numerical findings support the conjecture that the ratio is kept in favor of the inhibitor as usually.

The current contribution is a pioneering study of localized patterns in a fully nonlinear regime with Lévy flights. In §2 slowly drifting spikes are constructed. Their tail asymptotics is shown to be algebraic rather than exponential. The spike shape is determined by a solution to a fractional differential equation, analyzed in §3. In §4 a new type of a nonlocal eigenvalue problem with a fractional linear operator in addition to the usual nonlocality is posed. To solve this problem numerically a special numerical approach is devised (by contrast to a similar study with sub-diffusion [15], where the results obtained for regular diffusion could be used).

2. Quasi-equilibrium pattern

Equation (2a) possesses the background solution $a(x,t)\equiv 0$. Consider a solution of (2a) that is zero everywhere but at a finite set of locations x_i, $i=\{0,\dots,n-1\}$, the spikes' foci. Then an inner layer is formed near each focus with the spatial scaling given by

$$y_i(t) \stackrel{\text{def}}{=} \frac{x-x_i(\tau)}{\epsilon}, \quad i=\{0,\dots,n-1\}, \tag{3}$$

where τ is a slow evolution scale. The existence of a quasi-equilibrium spike-type solution is proved in the proposition below preceded by auxiliary lemmata.

LEMMA 1. *Let $u(y)$ be the least energy solution of*

$$\mathfrak{D}^\gamma_{|y|}u - u + u^p = 0 \quad -\infty < y < \infty, \quad u'(0)=0,\ u(0)>0, \quad \lim_{|y|\longrightarrow\infty} u = 0 \tag{4}$$

with $1\le\gamma<2$ and $p>1$. Then, the linearized operator $\mathcal{L}_0 = \mathfrak{D}^\gamma_{|y|} - 1 + pu^{p-1}$ in $\mathcal{L}_0 w = 0$ endowed with the boundary condition $\lim_{|y|\longrightarrow\infty} w = 0$ has dim Ker $\mathcal{L}_0 = 1$ *and* Ker $\mathcal{L}_0 = \{u'\}$.

Proof. The existence of the homoclinic solution $u(y)$ was proved in the study of ground state solutions to the equation $(-\Delta)^s Q + Q - Q^{\alpha+1} = 0$ with the range of the parameters s and α containing the sets relevant here [11]. Use the first equality in Definition 2

$$\mathfrak{D}^{\gamma}_{|y|}u'(y) = -\frac{\sec\widetilde{\gamma}}{2\Gamma(2-\gamma)}\frac{d^2}{dy^2}\left\{\int_{-\infty}^{y}\frac{u'(\xi)}{(y-\xi)^{\gamma-1}}\,d\xi + \int_{y}^{\infty}\frac{u'(\xi)}{(\xi-y)^{\gamma-1}}\,d\xi\right\},$$

perform integration by parts and differentiate the braced expression once to establish that

$$\mathfrak{D}^{\gamma}_{|y|}u'(y) = \frac{d}{dy}\mathfrak{D}^{\gamma}_{|y|}u(y)$$

by the second equality of Definition 2. Thus

$$\mathcal{L}_0 u' = \frac{d}{dy}\left(\mathfrak{D}^{\gamma}_{|y|}u - u + u^p\right) = 0,$$

and $u' \in \mathrm{Ker}\ \mathcal{L}_0$. The statement $\dim \mathrm{Ker}\ \mathcal{L}_0 = 1$ was proved by uniqueness considerations for a more general class of problems [11]. ■

Remark 1. Hereinafter the least energy solution to (4) will be referred to as the homoclinic for convenience. For $\gamma = 2$ this solution constitutes indeed the unique homoclinic.

LEMMA 2. *Let $u(y)$ be the solution of (4). Then $\mathcal{L}_0 = \mathfrak{D}^{\gamma}_{|y|} - 1 + pu^{p-1}$ in $\mathcal{L}_0 w = 0$ endowed with the boundary condition $\lim_{|y|\to\infty} w = 0$ is self-adjoint.*

Proof. Use the second equality in Definition 2 to obtain

$$\left\langle \mathfrak{D}^{\gamma}_{|y|}f_1, f_2\right\rangle = \frac{\sec\widetilde{\gamma}}{2\Gamma(-\gamma)}\int_{-\infty}^{\infty} f_2(y)\left\{\int_{-\infty}^{y}\frac{f_1(y)-f_1(\xi)}{(y-\xi)^{\gamma+1}}\,d\xi + \int_{y}^{\infty}\frac{f_1(y)-f_1(\xi)}{(\xi-y)^{\gamma+1}}\,d\xi\right\}dy,$$

swap the order of integration for $f_1(\xi)$ in each integral and then rename the variables $y \longleftrightarrow \xi$ to obtain

$$\left\langle \mathfrak{D}^{\gamma}_{|y|}f_1, f_2\right\rangle = \left\langle f_1, \mathfrak{D}^{\gamma}_{|y|}f_2\right\rangle.$$ ■

Remark 2. The solution $u(y)$ to the fractional equation $\mathfrak{D}^{\gamma}_{|y|}u - u + u^p = 0$ is not known exactly for any $1 < \gamma < 2$. For $\gamma = 2$ (regular diffusion) the

solution is given by [11]

$$u(y) = \left\{ \frac{p+1}{2} \operatorname{sech}^2 \left(\frac{p-1}{2} y \right) \right\}^{1/(p-1)}.$$

For $\gamma = 1$ (fastest Lévy flight) the solution is known only for $p = 2$ and is given by [11]

$$u(y) = \frac{2}{1+y^2}. \tag{5}$$

When $1 \leq \gamma < 2$, the decay of $u(y)$ at $|y| \longrightarrow \infty$ is no longer exponential. In the construction of spike-type solutions to (2) $u(y)$ will be related to the spikes' shape. Thus, a rigorous re-establishing of the proper localization of the spikes' foci is required, which in turn demands an insight into the asymptotics of u at $|y| \longrightarrow \infty$. The following two lemmata provide these results.

LEMMA 3. *Let $u(y)$ be the least energy solution of (4). Then for $1 \leq \gamma < 2$ and some $\mathfrak{a}(p, \gamma) > 0$*

$$u \sim -\frac{\mathfrak{a}(p,\gamma) \sec \widetilde{\gamma}}{2\Gamma(-\gamma)} |y|^{-(\gamma+1)} \quad |y| \gg 1, \quad \widetilde{\gamma} = \frac{\pi\gamma}{2}.$$

Proof. At $|y| \longrightarrow \infty$ $u^p \ll u$ holds and

$$\mathfrak{D}^{\gamma}_{|y|} u - u = -u^p \approx -\delta(\mathfrak{a}(p,\gamma) y).$$

The δ-function represents the far field and $\mathfrak{a}(p, \gamma)$ is the appropriate p-dependent weight. Thus after Fourier transform

$$\hat{u} = \frac{\mathfrak{a}(p,\gamma)}{1+|q|^{\gamma}},$$

and in the limit of small q (conforming to large $|y|$)

$$\begin{aligned} u \sim & \frac{\mathfrak{a}(p,\gamma)}{2\pi} \lim_{\varepsilon \longrightarrow 0} \int_{-\infty}^{\infty} e^{\imath qy - \varepsilon|q|} (1 - |q|^{\gamma} + \mathcal{O}\left(|q|^{2\gamma}\right)) dq \sim \mathfrak{a}(p,\gamma)\delta(y) \\ & - \frac{\mathfrak{a}(p,\gamma)}{\pi} \lim_{\varepsilon \longrightarrow 0} \int_0^{\infty} e^{-\varepsilon q} \cos(qy) q^{\gamma} dq. \end{aligned} \tag{6}$$

Here ε is not related to the activator diffusivity ϵ^{γ}. Note that

$$\int_0^{\infty} e^{-\varepsilon q} \cos(qy) q^{\gamma} dq = \Re \int_0^{\infty} e^{\imath qy - \varepsilon q} q^{\gamma} dq,$$

where $\Re$ denotes the real part. Construct a contour in the complex plane consisting of a sector of radius R in the first quadrant, bounded by the real

axis and the line $q = \varpi/(\varepsilon - \imath y)$. The integrand is analytic and by the residue theorem one obtains

$$\lim_{\substack{R\longrightarrow\infty\\ \varepsilon\longrightarrow 0}} \left\{ \int_0^R e^{\imath qy-\varepsilon q} q^\gamma\, dq + \int_0^{arctg(y/\varepsilon)} e^{(\imath y-\varepsilon)Re^{\imath\vartheta}} R^{1+\gamma} e^{(\gamma+1)\imath\vartheta}\, \imath\, d\vartheta \right.$$

$$\left. -\frac{1}{(\varepsilon-\imath y)^{\gamma+1}} \int_0^{R(\varepsilon^2+y^2)^{1/2}} e^{-\varpi}\varpi^\gamma\, d\varpi \right\} = 0.$$

The integral along the arc vanishes because $0 \le \vartheta < \frac{\pi}{2}$. Thus

$$\lim_{\varepsilon\longrightarrow 0} \Re \int_0^\infty e^{\imath qy-\varepsilon q} q^\gamma\, dq = -\frac{\Gamma(\gamma+1)}{y^{\gamma+1}} \sin\widetilde{\gamma} = \frac{\pi \sec\widetilde{\gamma}}{2\Gamma(-\gamma) y^{\gamma+1}},$$

where the following identity was used

$$\Gamma(\gamma+1) = -\frac{\pi \csc(\pi\gamma)}{\Gamma(-\gamma)}.$$

Finally, from (6) along with the fact $u(y)$ is an even function by (4),

$$u \sim -\frac{\mathfrak{a}(p,\gamma)\sec\widetilde{\gamma}}{2\Gamma(-\gamma)}\ |y|^{-(\gamma+1)}, \quad |y| \gg 1.$$

Because $\mathfrak{a}(p,\gamma)$ is not known, only the algebraic decay rate of the asymptotics can be used. The constant cannot be determined because this is in fact a solution to the linearized problem. ■

Remark 3. For $\gamma = 1$ and $p = 2$ by the exact solution (5) $u \sim 2y^{-2}$ when $|y| \gg 1$, and thus the factor $\mathfrak{a}(p,\gamma)$ becomes

$$\mathfrak{a}(2,1) = -\lim_{\gamma\longrightarrow 1^+} 4\Gamma(-\gamma)\cos\widetilde{\gamma} = 2\pi.$$

LEMMA 4. *At the limit $\epsilon \longrightarrow 0$ the expression of the form a^r/ϵ for any $r > 0$ and a localized function $a(x,t)$ given by*

$$a(x,t) \sim \sum_{i=0}^{n-1} \alpha_i(\tau) u\left(\frac{x-x_i}{\epsilon}\right)$$

conforms to a generalized function of the Dirac delta type, satisfying

$$\lim_{\epsilon\longrightarrow 0} \epsilon^{-1} \int_{x_0}^{x_0+\delta x} a^r\, dx = 0 \quad \forall \quad |x_0 - x_i| \gg \delta x \sim \mathcal{O}(\epsilon), \tag{7a}$$

$$\lim_{\epsilon\longrightarrow 0} \epsilon^{-1} \int_{x_i^-}^{x_i^+} a^r\, dx \sim \mathcal{O}(1). \tag{7b}$$

Proof. Use the form of a to obtain (7a) by a direct computation:

$$\lim_{\epsilon \longrightarrow 0} \epsilon^{-1} \int_{x_0}^{x_0+\delta x} a^r \, dx \sim \lim_{\epsilon \longrightarrow 0} \int_{(x_0-x_i)/\epsilon}^{(\delta x+x_0-x_i)/\epsilon} \left(\sum_{i=0}^{n-1} \alpha_i u(\zeta) \right)^r d\zeta = 0.$$

The last equality ensues due to the following facts

$$\lim_{\epsilon \longrightarrow 0} \frac{x_0 - x_i}{\epsilon} = \infty \cdot \operatorname{sgn}(x_0 - x_i), \quad \frac{\delta x}{\epsilon} \sim \mathcal{O}(1), \quad \lim_{|\zeta| \longrightarrow \infty} u(\zeta) = 0.$$

Note that u can be any function decaying at infinity. Thus (7a) is proved. To show (7b), change the integration variable to y_i

$$\lim_{\epsilon \longrightarrow 0} \epsilon^{-1} \int_{x_i^-}^{x_i^+} a^r \, dx \sim \alpha_i \int_{-\infty}^{\infty} u^r (y_i) \, dy_i \sim \mathcal{O}(1),$$

where the passage to the inner layer of the i-th spike uses the assumption on sufficient decay (no longer exponential) of the contributions of the adjacent and farther spikes as well as the integrability of u^r (for the homoclinic (4) the integrability ensues by Lemma 3). ■

PROPOSITION 1. *Let $x_i(\tau)$ be the location of the center of the ith spike, evolving on the slow time scale $\tau = \epsilon^2 t$. Suppose that $\tau_o \sim o(\epsilon^{-2})$. Then at the limit $\epsilon \longrightarrow 0$ in each inner region the quasi-equilibrium solution of (2) is given asymptotically by*

$$A(y_i, \tau) = a(x_i + \epsilon y_i, \epsilon^{-2}\tau) = A_i^{(0)} + \epsilon A_i^{(1)} + \ldots \tag{8a}$$

$$H(y_i, \tau) = h(x_i + \epsilon y_i, \epsilon^{-2}\tau) = H_i^{(0)} + \epsilon H_i^{(1)} + \ldots, \tag{8b}$$

where

$$H_i^{(0)} = \bar{H}_i(\tau), \quad A_i^{(0)} = \bar{H}_i^{\beta} u(y_i), \quad \beta = \frac{q}{p-1},$$

$u(y)$ is the solution of (4) and

$$\bar{H}_i(\tau) = -b_m \sum_{j=0}^{n-1} \bar{H}_j^{\beta m - s} G(x_i; x_j), \quad b_m = \int_{-\infty}^{\infty} u^m \, dy \tag{9a}$$

$$\frac{dx_i}{d\tau} = \frac{q \, b_m f(p)}{(p+1)\bar{H}_i} \left\{ \sum_{\substack{j=0 \\ j \neq i}}^{n-1} \bar{H}_j^{\beta m - s} G'(x_i; x_j) + \frac{1}{2} \bar{H}_i^{\beta m - s} (G'(x_i^-; x_i) + G'(x_i^+; x_i)) \right\}$$

$$f(p) = \int_{-\infty}^{\infty} u^{p+1} dy \Big/ \int_{-\infty}^{\infty} u'^2 \, dy. \tag{9b}$$

In (9) $G(x;x_i)$ is the Green's function satisfying

$$DG'' - \mu G = \delta(x - x_i), \quad G'(\pm 1; x_i) = 0.$$

Proof. Substitution of (8) into (2) gives the following system for the leading order functions

$$\left(\mathfrak{D}^{\gamma}_{|y_i|} - 1\right) A_i^{(0)} + \frac{A_i^{(0)p}}{H_i^{(0)q}} = 0, \quad -\infty < y < \infty, \tag{10a}$$

$$\lim_{|y_i| \longrightarrow \infty} \frac{\partial A_i^{(0)}}{\partial y_i} = 0,$$

$$\frac{\partial^2}{\partial y_i^2} H_i^{(0)} = 0, \quad -\infty < y < \infty, \tag{10b}$$

$$\lim_{|y_i| \longrightarrow \infty} \frac{\partial H_i^{(0)}}{\partial y_i} = 0.$$

The correction equations are

$$\left(\mathfrak{D}^{\gamma}_{|y_i|} - 1\right) A_i^{(1)} + p \frac{A_i^{(0)p-1}}{H_i^{(0)q}} A_i^{(1)} = q \frac{A_i^{(0)p}}{H_i^{(0)q+1}} H_i^{(1)} - \frac{dx_i}{d\tau} \frac{\partial}{\partial y_i} A_i^{(0)}, \tag{11a}$$
$$-\infty < y < \infty,$$

$$\lim_{|y_i| \longrightarrow \infty} \frac{\partial A_i^{(1)}}{\partial y_i} = 0.$$

$$D \frac{\partial^2}{\partial y_i^2} H_i^{(1)} = -\frac{A_i^{(0)m}}{H_i^{(0)s}}, \quad -\infty < y < \infty, \tag{11b}$$

$$\lim_{|y_i| \longrightarrow \infty} \frac{\partial H_i^{(1)}}{\partial y_i} = 0.$$

Solving (10b) gives $H_i^{(0)} = \bar{H}_i(\tau)$. Proposing $A_i^{(0)} = \bar{H}_i^{\beta} u(y_i)$ gives $\beta = \frac{q}{p-1}$ and $\mathfrak{D}^{\gamma}_{|y_i|} u - u + u^p = 0$. With this (11a) is re-written as

$$\mathcal{L}_0 A_i^{(1)} = q \bar{H}_i^{\beta-1} u^p H_i^{(1)} - \bar{H}_i^{\beta} u'(y_i) \frac{dx_i}{d\tau}, \quad \mathcal{L}_0 = \mathfrak{D}^{\gamma}_{|y_i|} - 1 + p u^{p-1}.$$

Thus by the Fredholm alternative ($\mathcal{L}_0$ is self-adjoint by Lemma 2) one gets

$$\frac{q}{\bar{H}_i}\int_{-\infty}^{\infty} u' u^p H_i^{(1)} dy_i = \frac{dx_i}{d\tau}\int_{-\infty}^{\infty} u'^2 dy_i,$$

which can be shown to give (same as for regular diffusion [12])

$$\frac{q}{2(p+1)\bar{H}_i}\int_{-\infty}^{\infty} u^{p+1} dy_i \left(\lim_{y_i \longrightarrow \infty} \frac{dH_i^{(1)}}{dy_i} + \lim_{y_i \longrightarrow -\infty} \frac{dH_i^{(1)}}{dy_i}\right) = \frac{dx_i}{d\tau}\int_{-\infty}^{\infty} u'^2 dy_i\,. \tag{12}$$

For the outer solution expand

$$h(x,t) \sim h^{(0)}(x,t) + \mathcal{O}(\epsilon).$$

Then the matching to the inner solution yields

$$h^{(0)}(x_i,t) = \bar{H}_i(\tau)$$

$$\lim_{y_i \longrightarrow \pm\infty} \frac{dH_i^{(1)}}{dy_i} = \lim_{\substack{y_i \longrightarrow \pm\infty \\ \epsilon \longrightarrow 0}} \epsilon^{-1}\frac{\partial}{\partial y_i}\left(h\left(x_i + \epsilon y_i, \epsilon^{-2}\tau\right) - H_i^{(0)}\right) = \lim_{x \longrightarrow x_i^{\pm}} \frac{\partial h^{(0)}}{\partial x}. \tag{13}$$

By Lemma 4 the nonlinear term of (2b) can be expressed as a combination of δ-functions due to the localized behavior of a

$$\epsilon^{-1}\frac{a^m}{h^s} = \sum_{i=0}^{n-1} b_i\,\delta(x - x_i).$$

Then integrating over $[x_i^-\,,\ x_i^+]$ it is found that the weights are identical for all the spikes

$$b_i = \epsilon^{-1}\int_{x_i^-}^{x_i^+} \frac{a^m}{h^s}\,dx = \int_{-\infty}^{\infty} \frac{a^m}{h^s}\,dy_i = \bar{H}_i^{\beta m - s}\int_{-\infty}^{\infty} u^m\,dy_i.$$

From (2b) the equation for $h^{(0)}$ is

$$Dh_{xx}^{(0)} - \mu h^{(0)} = -b_m \sum_{i=1}^{n} \bar{H}_i^{\beta m - s}\delta(x - x_i), \quad h_x^{(0)}(\pm 1) = 0, \quad b_m = \int_{-\infty}^{\infty} u^m\,dy.$$

The solution in terms of Green's function is

$$h^{(0)}(x,t) = -b_m \sum_{i=1}^{n} \bar{H}_i^{\beta m - s} G(x; x_i), \quad DG' - \mu G = \delta(x - x_i), \quad G'(\pm 1; x_i) = 0. \tag{14}$$

The contribution of the temporal term is negligible at this order because $\tau_o \partial_t h^{(0)} = \tau_o \epsilon^2 \partial_\tau h^{(0)} \sim o(\epsilon)$, and the only dependence on t comes through $\bar{H}_i(\tau)$ (same as for regular diffusion). Using $h^{(0)}(x,t)$ in the matching conditions (13) and the solvability condition (12) yields the desired differential-algebraic system. ■

Remark 4. The differential-algebraic system (9) has the same form as its counterpart for regular diffusion and exhibits no explicit dependence on the anomaly exponent γ as an additional parameter. The dependence on γ comes through the homoclinic u, i.e. only the factors $f(p)$ and b_m change.

3. Computation of homoclinic

3.1. Numerical solution

Due to the nonlocality of the fractional Laplacian the implementation of numerical schemes is significantly easier in Fourier space, where the computation of $(-\Delta)^{\gamma/2}$ is straightforward with Definition 4. However, solving an equation of the type (4) in Fourier space requires iteration at each point of the grid due to its nonlinearity. A few iterative methods were tested (simple iteration, secant) and exhibited no convergence even when the initial function was very close to the true solution (cases $\gamma = 1$ and $\gamma = 2$ with $p = 2$).

On the other hand, because (4) locally minimises a functional, the homoclinic is a steady state of a scalar partial differential equation. However, this steady state solution is unstable similarly to the regular diffusion case owing to the strictly positive eigenvalue of the linearized operator $\mathcal{L}_0 = \mathfrak{D}^{\gamma}_{|y|} - 1 + pu^{p-1}$ (by Lemma 1 zero is an eigenvalue for all γ with u' being the eigenfunction, and by Sturm-Liouville theory for $\gamma = 2$ this immediately implies a strictly positive eigenvalue with an eigenfunction that does not change sign). In the case of the shadow model [16] a system of two PDEs was used to obtain the homoclinic as a stable steady state in the limit $D \longrightarrow \infty$. A similar approach was adopted in the present work, and the following simplified system was solved

$$\begin{aligned} \mathfrak{u}_t &= \epsilon^{\gamma} \mathfrak{D}^{\gamma}_{|x|} \mathfrak{u} - \mathfrak{u} + \frac{\mathfrak{u}^p}{\mathfrak{v}}, \\ \tau_o \mathfrak{v}_t &= D\, \mathfrak{v}_{xx} - \mathfrak{v} + \frac{\mathfrak{u}^p}{\epsilon}. \end{aligned} \tag{15}$$

The scheme was pseudo-spectral, i.e. the system

$$\begin{aligned} \frac{d\widehat{\mathfrak{u}}}{dt} &= -(\epsilon^{\gamma}|q|^{\gamma} + 1)\widehat{\mathfrak{u}} + \mathcal{F}\left\{\frac{\mathfrak{u}^p}{\mathfrak{v}}\right\}, \\ \frac{d\widehat{\mathfrak{v}}}{dt} &= -(Dq^2 + 1)\widehat{\mathfrak{v}} + \mathcal{F}\left\{\frac{\mathfrak{u}^p}{\epsilon}\right\}, \end{aligned} \tag{16}$$

where the hats denote Fourier transformed quantities, was integrated in time with the Euler method.

The linear terms were integrated by the implicit Crank–Nicolson scheme, whereas for the nonlinear terms the explicit Adams–Bashforth scheme was employed. The parameters used in the computation were as follows. The

anomaly exponent was $1 \leq \gamma \leq 2$. The homoclinic nonlinearity p was chosen as two rather common values $p = 2$ and $p = 3$. The spatial domain was $x \in [-2\pi, 2\pi)$. The remaining parameters were the time step $\delta t = 0.01$, number of Fourier modes $N = 2048$, inhibitor diffusivity $D = 1000$, activator diffusivity $\epsilon = 0.1$, characteristic time $\tau_o = 0.2$ for $p = 2$ and $\tau_o = 0.1$ for $p = 3$. The choice of τ_o affects greatly the stability of the solution, and the values were chosen significantly below the thresholds known for Hopf bifurcations in the case of regular diffusion [16]. For higher values of p the required value is $\tau_o \ll 1$, which requires a very small time step (similarly to regular diffusion). Because exact solutions are known for $\gamma = 2$ with all p and for $\gamma = 1,\ p = 2$, these are interpolated to assign the initial function for any desired γ and p.

For $D \gg 1$ the asymptotic solution is expected to be in the form

$$\mathfrak{u} \sim \mathfrak{u}_0 + \frac{\mathfrak{u}_1}{D} + \mathcal{O}\left(\frac{1}{D^2}\right), \quad \mathfrak{v} \sim \mathfrak{v}_0 + \frac{\mathfrak{v}_1}{D} + \mathcal{O}\left(\frac{1}{D^2}\right).$$

For the inhibitor at $\mathcal{O}(D)$ $\mathfrak{v}_{0xx} = 0$, giving $\mathfrak{v}_0 = \mathfrak{v}_0(t)$ to have no flux at the boundary. At $\mathcal{O}(1)$

$$\mathfrak{v}_{1xx} = \tau_o \mathfrak{v}_{0t} + \mathfrak{v}_0 - \frac{\mathfrak{u}_0^p}{\epsilon},$$

yielding the solvability condition

$$\mathfrak{v}_0 + \tau_o \mathfrak{v}_{0t} = \frac{1}{4\pi\epsilon} \int_{-2\pi}^{2\pi} \mathfrak{u}_0^p \, dx \quad \forall\, t, \qquad \mathfrak{v}_0 = \frac{1}{4\pi\epsilon} \int_{-2\pi}^{2\pi} \mathfrak{u}_0^p \, dx = \text{const} \quad t \longrightarrow \infty.$$

For the activator at $\mathcal{O}(1)$

$$\mathfrak{u}_{0t} = \epsilon^\gamma \mathfrak{D}_{|x|}^\gamma \mathfrak{u}_0 - \mathfrak{u}_0 + \frac{\mathfrak{u}_0^p}{\mathfrak{v}_0}$$

and at $t \longrightarrow \infty$

$$\epsilon^\gamma \mathfrak{D}_{|x|}^\gamma \mathfrak{u}_0 - \mathfrak{u}_0 + \frac{\mathfrak{u}_0^p}{\mathfrak{v}_0} = 0$$

or using $y = x/\epsilon$

$$\mathfrak{D}_{|y|}^\gamma \mathfrak{u}_0 - \mathfrak{u}_0 + \frac{\mathfrak{u}_0^p}{\mathfrak{v}_0} = 0.$$

Because at the steady state $\mathfrak{v}_0$ is constant, rescaling $\mathfrak{u}_0 = \mathfrak{a}\, u$ gives $\mathfrak{a} = \mathfrak{v}_0^{1/(p-1)}$ for the sought homoclinic that solves (4).

For the inhibitor zero flux boundary conditions are implemented with the simplest first order forward and backward differences, i.e. setting the grid to $x_j = 4\pi(j - N/2)/N,\ j = 0, \ldots, N-1$ and $\delta x = 4\pi/N$, the boundary

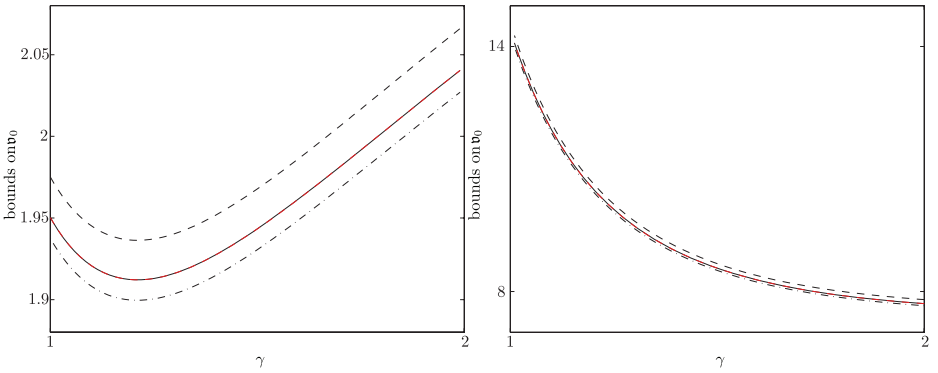

Figure 1. Verification of the asymptotic solvability condition at steady state $\mathfrak{v}_0 = \frac{1}{4\pi\epsilon}\int_{-2\pi}^{2\pi} \mathfrak{u}_0^p\, dx$ for $p = 2$ (left) and $p = 3$ (right): integration of $\mathfrak{u}$ and mean value of $\mathfrak{v}$ (solid black and red/gray curves, difference indistinguishable), $\max_x \mathfrak{v}$ (dashed curve) and $\min_x \mathfrak{v}$ (dash-dotted curve).

conditions are $\mathfrak{v}(x_0) = \mathfrak{v}(x_1)$ and $\mathfrak{v}(x_{N-1}) = \mathfrak{v}(x_{N-2})$. For the activator it is necessary to enforce the correct algebraic decay. By Lemma 3 at $t \longrightarrow \infty$

$$\frac{\mathfrak{u}'}{\mathfrak{u}} = -\frac{\gamma+1}{x},$$

disretized using forward differences to give

$$\frac{\mathfrak{u}(x_{j+1}) - \mathfrak{u}(x_j)}{\delta x\ \mathfrak{u}(x_j)} = -\frac{\gamma+1}{x_j}$$

or

$$\mathfrak{u}(x_{j+1}) = \mathfrak{u}(x_j)\left(1 - \frac{\gamma+1}{j - N/2}\right).$$

This condition was implemented at the penultimate three points of the right tail and reflected to the left tail (conforming to backward differences there).

In addition to the reconstruction of exact solutions some precision checks were performed for the parameters p and γ, where exact solutions were not known. Figure 1 compares the quantities involved in the asymptotic solvability condition with the numerical values of v and u. Figure 2 depicts the least squares fit slope of numerically obtained $\ln u$ with the expected line $-(\gamma+1)$.

3.2. Hopf bifurcation threshold for τ_o

The homoclinic code allows to obtain an interesting related result. As mentioned in §3.1, if the value of τ_o is not taken sufficiently small, the convergence to the homoclinic is oscillatory and slow, and when crossing a critical threshold of τ_o, no homoclinic is obtained. The computation of the threshold value τ_{th} was done for the same value of D as for the homoclinics. The value of τ_o was given as before until the convergence of the homoclinic maximum point to seven

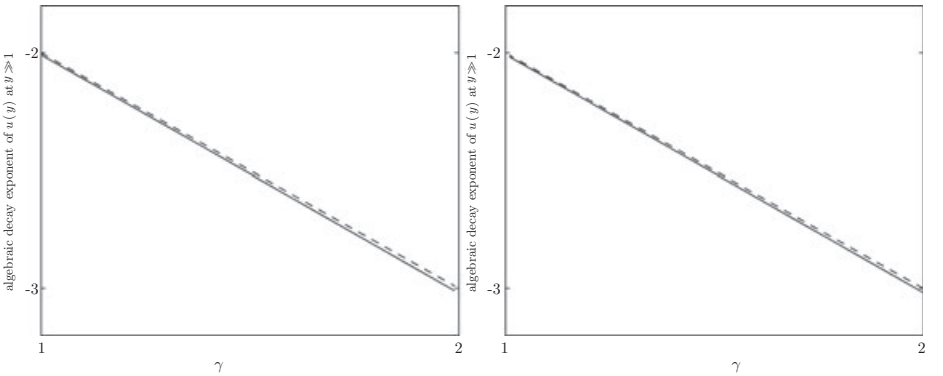

Figure 2. Comparison of the algebraic decay exponent for $p = 2$ (left) and $p = 3$ (right) of numerically computed homoclinics $\mathfrak{u}$ (solid) and the asymptotic exponent $-(\gamma + 1)$ (dashed).

significant digits, then τ_o was increased by increments of 0.001 to a value slightly below the threshold, while watching for further convergence of the homoclinic maximum to eleven significant digits. Then τ_o was increased by increments of 0.00002 past the threshold, and the simulation was stopped when the relative change in the maximal value exceeded one order of magnitude. Starting at $\gamma = 1$, at each value of γ the obtained τ_{th} was used as the new initial guess for the next value of γ (incremented by 0.01 till $\gamma = 2$). Figure 3 shows typical pictures of the developing instability. Figure 4 shows a less typical picture of beats seen around $\gamma = 1.2$. Apparently two unstable eigenvalues interact there. Note how the frequency of the oscillation increases from $\gamma = 1$ till beats appear, then at $\gamma = 1.3$ the beats are almost indistinguishable, and past $\gamma = 1.3$ the frequency decreases again. Also, as γ approaches the normal value $\gamma = 2$, the instability is more pronounced, i.e. the oscillation amplitude develops faster.

Figure 5 shows the threshold value τ_{th} versus the anomaly exponent γ. The dependence is slightly nonlinear and the slope grows steeper as γ becomes more anomalous.

4. Eigenvalue problem

By Proposition 1 the uniformly valid form of the quasi-equilibrium spike pattern is

$$a_{\text{qe}} = \sum_{i=0}^{n-1} \bar{H}_i^{\beta}\, u\left(\frac{x - x_i}{\epsilon}\right),$$

$$h_{\text{qe}} = -b_m \sum_{i=0}^{n-1} \bar{H}_i^{\beta m - s}\, G(x; x_i).$$

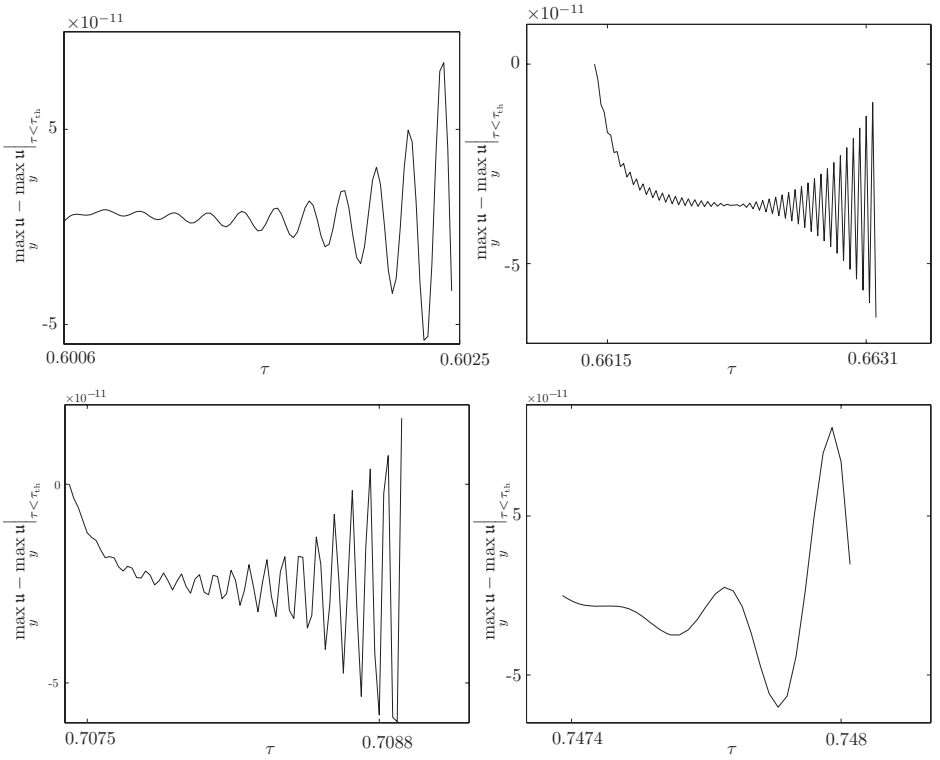

Figure 3. Divergence of $\max_y \mathrm{u}$ at the Hopf bifurcation threshold τ_{th} for $p = 2$ and $\gamma = 1$ (left upper), $\gamma = 1.2$ (right upper), $\gamma = 1.4$ (left lower), $\gamma = 1.6$ (right lower).

Because the temporal derivative in (2) is of an integer order, a proper spectrum is expected (as opposed to a sub-diffusive system with a fractional temporal derivative, where exponential perturbations cannot evolve with a constant growth rate [15]). The theorem below gives the ensuing nonlocal eigenvalue problem.

THEOREM 1. *The eigenfunction* $\tilde{a}(x)$ *of the eigenpair* $\{\lambda, \tilde{a}(x)\}$ *in*

$$a \sim a_{\mathrm{qe}} + e^{\lambda t}\tilde{a}(x), \quad h \sim h_{\mathrm{qe}} + e^{\lambda t}\tilde{h}(x), \quad |\tilde{a}(x)|, |\tilde{h}(x)| \sim o(1)$$

is of the form

$$\tilde{a} \sim \sum_{i=0}^{n-1} \tilde{a}_i \left(\frac{x - x_i}{\epsilon}\right), \tag{17}$$

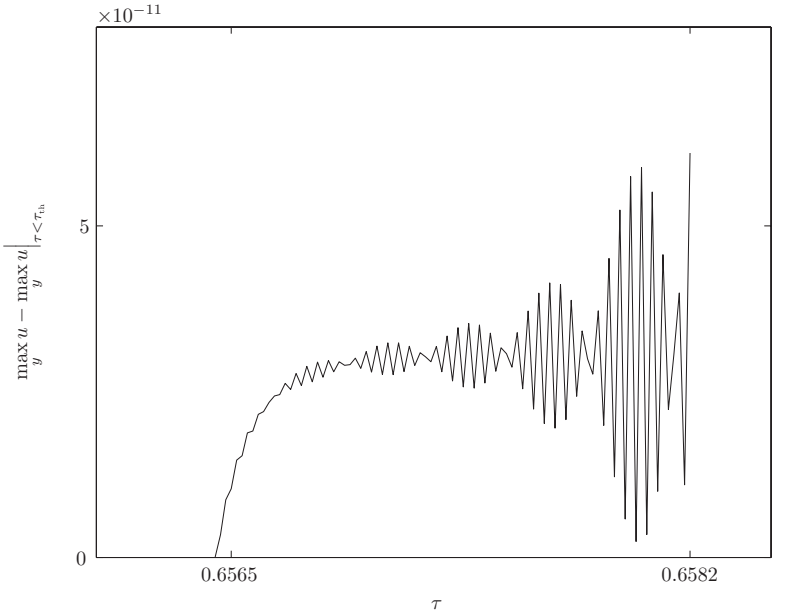

Figure 4. Divergence of $\max_y \mathfrak{u}$ at the Hopf bifurcation threshold τ_{th} for $\gamma = 1.18$, $p = 2$: the phenomenon of beats.

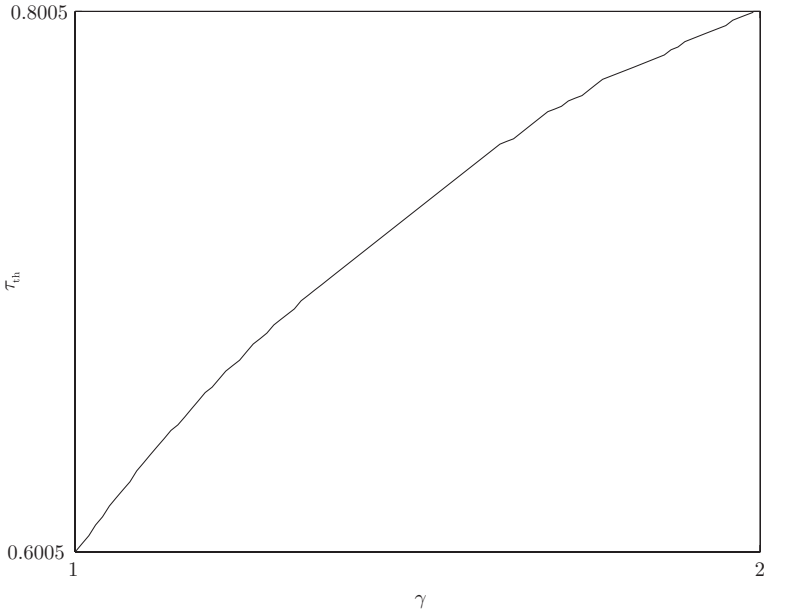

Figure 5. Hopf bifurcation threshold τ_{th} versus γ for $p = 2$.

where $\{\lambda, \tilde{a}_i\}$ *is the solution of the nonlocal problem in the vicinity of the* i*-th spike*

$$\mathfrak{D}^{\gamma}_{|y_i|}\tilde{a}_i - (1 + \lambda - pu^{p-1})\tilde{a}_i = q\,\bar{H}_i^{\beta-1}u^p\tilde{h}\,(x_i)\,, \quad i = \{0, \ldots, n-1\}.$$

Proof. Upon linearization for the eigenfunctions $\tilde{a}$ and $\tilde{h}$ system (2) reads

$$\lambda\,\tilde{a} = \epsilon^{\gamma}\mathfrak{D}^{\gamma}_{|x|}\tilde{a} - \tilde{a} + p\frac{a_{\mathrm{qe}}^{p-1}}{h_{\mathrm{qe}}^{q}}\tilde{a} - q\frac{a_{\mathrm{qe}}^{p}}{h_{\mathrm{qe}}^{q+1}}\tilde{h}, \tag{18a}$$

$$\tau_0\,\lambda\,\tilde{h} = D\,\frac{d^2\tilde{h}}{dx^2} - \mu\tilde{h} + \frac{m}{\epsilon}\frac{a_{\mathrm{qe}}^{m-1}}{h_{\mathrm{qe}}^{s}}\tilde{a} - \frac{s}{\epsilon}\frac{a_{\mathrm{qe}}^{m}}{h_{\mathrm{qe}}^{s+1}}\tilde{h}, \tag{18b}$$

$$\left.\frac{d}{dx}\tilde{a}\right|_{x=\pm1} = \left.\frac{d}{dx}\tilde{h}\right|_{x=\pm1} = 0. \tag{18c}$$

Seeking an eigenfunction of the form (17) and expressing all terms of the type a^r/ϵ in (18b) according to Lemma 4 yields the desired eigenvalue problem with the boundary conditions $\lim_{|y_i|\longrightarrow\infty}\tilde{a}_i = 0$ replacing (18c). ■

COROLLARY 1. *For a pattern of* n *spikes with identical height the eigenfunction is*

$$\tilde{a} \sim \sum_{i=0}^{n-1} c_i\,\tilde{A}\left(\frac{x - x_i}{\epsilon}\right), \quad c_i = const,$$

where $\tilde{A}(y)$ *is the solution to*

$$\mathfrak{D}^{\gamma}_{|y|}\tilde{A} - (1 + \lambda - pu^{p-1})\tilde{A} = \frac{\chi u^p}{b_m}\int_{-\infty}^{\infty} u^{m-1}\tilde{A}\,dy,$$

$$\chi = qm\left(s + \frac{\nu}{2}\frac{\vartheta}{\vartheta_o}\,\mathrm{ctgh}\,\frac{\vartheta_o}{n}\right)^{-1},$$

$$\nu = \nu\,(\lambda; n, i) = \frac{2}{\sinh(2\vartheta/n)}\left(\cosh\frac{2\vartheta}{n} - \cos\frac{\pi i}{n}\right) \geq 0,$$

$$\vartheta = \sqrt{\frac{\mu + \tau_o\lambda}{D}}, \quad \vartheta_o = \sqrt{\frac{\mu}{D}}.$$

Proof. By Theorem 1 the eigenvalue problem for any spike pattern is identical to the case of regular diffusion but for the dependence on the solution to (4). The desired result was previously proved for regular diffusion [12, 14]. ■

Remark 5. The nonlocal eigenvalue problem in Corollary 1 can be also written in a vector form, allowing to relate the constants c_i to an eigenvector of a certain tridiagonal matrix [12, 14].

PROPOSITION 2. *For* $\lambda = 0$ *the solution of*

$$\mathfrak{D}^{\gamma}_{|y|}\tilde{A} - (1 + \lambda - pu^{p-1})\tilde{A} = \frac{\chi u^p}{b_m}\int_{-\infty}^{\infty} u^{m-1}\tilde{A}\,dy,$$

is $\tilde{A}(y) = u(y)/(p-1)$ *for all values of* γ *(up to a multiplicative constant).*

Proof. Due to the problem linearity $\tilde{A}$ can only be determined up to a multiple. Thus it suffices to consider

$$\mathfrak{D}^{\gamma}_{|y|}\tilde{A} - (1 - pu^{p-1})\tilde{A} = u^p,$$

i.e. set

$$\frac{\chi}{b_m}\int_{-\infty}^{\infty} u^{m-1}\tilde{A}\,dy = 1.$$

Substitutiting $\tilde{A}(y) = u(y)/(p-1)$ and using $\mathfrak{D}^{\gamma}_{|y|}u - u = -u^p$ completes the proof. ■

Combining Proposition 2 and Lemma 3, it is obvious that for $\lambda = 0$ and all values of γ the eigenfunction $\tilde{A}(y)$ is real and obeys the asymptotics $\tilde{A} \sim |y|^{-(\gamma+1)}$ as $|y| \gg 1$. The decay of $\tilde{A}(y)$ for any λ is required to set the proper boundary conditions in the course of a numerical solution of the eigenvalue problem in Corollary 1. The following proposition proves that the same asymptotics holds for all values of λ both for $\Re\tilde{A}$ and $\Im\tilde{A}$ (whenever $\Im\tilde{A} \not\equiv 0$).

PROPOSITION 3. *The solution* $\tilde{A}(y)$ *of*

$$\mathfrak{D}^{\gamma}_{|y|}\tilde{A} - (1 + \lambda - pu^{p-1})\tilde{A} = u^p, \qquad \lim_{|y|\longrightarrow\infty}\tilde{A}(y) = 0$$

where $\lambda = \lambda_r + \imath\lambda_i$ *with* $\lambda_r, \lambda_i \in \mathbb{R}$, *obeys the following asymptotics. If* $\lambda_i \neq 0$,

$$\Re\tilde{A} \sim |y|^{-(\gamma+1)}, \quad \Im\tilde{A} \sim |y|^{-(\gamma+1)} \quad \text{as} \quad |y| \longrightarrow \infty.$$

If $\lambda_i = 0$, $\Im\tilde{A} \equiv 0$ *and*

$$\Re\tilde{A} \sim |y|^{-(\gamma+1)} \quad \text{as} \quad |y| \longrightarrow \infty.$$

Proof. Because the problem stated in Corollary 1 is symmetric in y, both $\Re\tilde{A}(y)$ and $\Im\tilde{A}(y)$ are even functions. Thus it suffices to consider only $y > 0$. By Lemma 3 the linear terms in $\mathfrak{D}^{\gamma}_{|y|}u - u + u^p = 0$ are of order $\mathcal{O}(y^{-(\gamma+1)})$ and balance each other as $y \longrightarrow \infty$, whereas the nonlinear term is of order $\mathcal{O}(y^{-p(\gamma+1)})$ and is negligible. By an argument identical to that presented in Lemma 3 the decay of $\tilde{A}$ must be algebraic for any $1 \leq \gamma < 2$. Suppose $\Re\tilde{A} \sim y^{-\alpha_r}$ and $\Im\tilde{A} \sim y^{-\alpha_i}$ with $\alpha_r, \alpha_i > 0$. Then $u^{p-1}\Re\tilde{A} \sim \mathcal{O}(y^{-(p-1)(\gamma+1)-\alpha_r})$ is negligible as compared to the linear term $\Re\tilde{A}$, and the same holds for $\Im\tilde{A}$ with α_i. The remaining terms correspond exactly to the terms balanced by equation (4), because the presence of λ does not change their magnitude. Thus u^p can be represented by Dirac delta function as in Lemma 3, and the corresponding linear equations are given by

$$\mathfrak{D}^{\gamma}_{|y|}\Re\tilde{A} - (1 + \lambda_r)\Re\tilde{A} \sim \delta(y),$$

$$\mathfrak{D}^{\gamma}_{|y|}\Im\tilde{A} - \lambda_i\Im\tilde{A} \sim \delta(y).$$

An argument identical to Lemma 3 yields the desired asymptotics, i.e. $\alpha_r = \gamma + 1$ and $\alpha_i = \gamma + 1$ if $\lambda_i \neq 0$. If $\lambda_i = 0$, $\Im\tilde{A} \equiv 0$ because the problem is real. ■

4.1 Numerical solution of the eigenvalue problem for a single spike

To demonstrate the effect of Lévy flights on the location of the eigenvalues, the simplest case of a single spike was considered. Similarly to regular diffusion, the only exact solution known for the nonlocal eigenvalue problem is for $\lambda = 0$, and the problem must be solved numerically for any other value of λ. An elaborate numerical investigation of the possible spike patterns is beyond the scope of this paper. In this section, a few distinctive effects of Lévy flights are discussed. One of the desired results is the path followed by the eigenvalues in the right half plane, parametrized by τ_o and in particular the Hopf bifurcation threshold, i.e., the value of τ_o where the eigenvalue is purely imaginary. As a first step the linear problem (as in Proposition 3)

$$\mathfrak{D}^{\gamma}_{|y|}\tilde{A} - (1 + \lambda - pu^{p-1})\tilde{A} = u^p, \qquad \lim_{|y|\longrightarrow\infty} \tilde{A}(y) = 0,$$

is solved for a guessed range of $\Im\lambda$ with $\Re\lambda$ fixed. Then the transcedental equation for the normalization condition

$$\frac{\chi}{b_m}\int_{-\infty}^{\infty} u^{m-1}\tilde{A}\,dy = 1,$$

is solved to find $\Re\lambda$. This procedure is repeated for sufficiently dense values of $\Re\lambda$ to obtain the desired path. The detailed description of the discretization scheme and implementation appear in Appendix.

Table 1
Hopf Bifurcation Frequency and Corresponding Value of τ_o with Regular Diffusion (Courtesy of M. J. Ward).

(p, q, m, s)	D	$\Im\lambda\|_{\Re\lambda=0}$	$\tau_o\|_{\Re\lambda=0}$
(2,1,2,0)	0.5	0.8509	1.9934
	1.0	0.9678	1.3431
	1.5	1.0372	1.1346
(2,1,3,0)	0.5	0.9499	4.6229
	1.0	1.0746	2.4822
	1.5	1.2553	1.6932
(3,2,2,0)	0.5	2.0903	0.70241
	1.0	2.3284	0.49675
	1.5	2.4647	0.42858

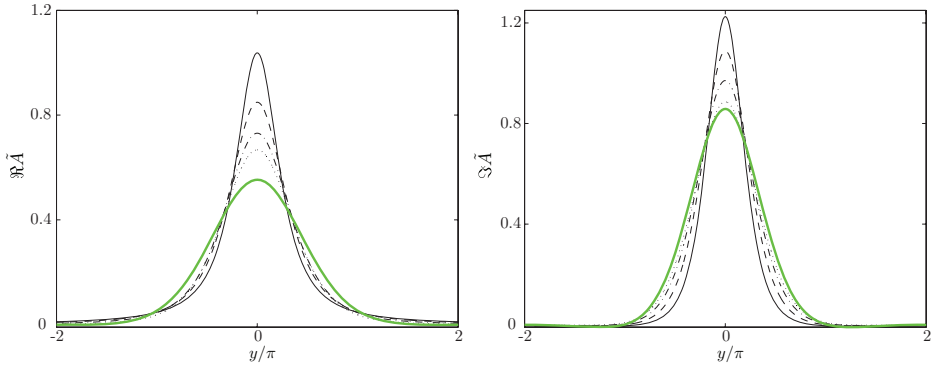

Figure 6. Eigenfunction $\tilde{A}$ for a single spike with the set of exponents $(p, q, m, s) = (2, 1, 2, 0)$, $\lambda = 1.6667\,\imath$ and the anomaly exponents $\gamma = 1.05$ (solid), $\gamma = 1.25$ (dashed), $\gamma = 1.5$ (dash-dotted) and $\gamma = 1.75$ (dotted) compared to regular diffusion ($\gamma = 2$, thick green/gray curves, courtesy of M. J. Ward).

The solution code was tested in the case $\lambda = 0$ to yield an eigenfunction consistent with the exact solution from Proposition 2 for all $1 \leq \gamma < 2$. It was impossible to reproduce directly the results of regular diffusion with this code because Definition 2 and the discretization procedure are not valid for $\gamma = 2$. Moreover, the evaluation of the principal value integrals becomes extremely challenging as $\gamma \longrightarrow 2^-$. With the current numerical method the eigenvalue problem can be solved for $1 < \gamma \leq 1.75$, and the precision deteriorates quickly for $1.75 < \gamma < 2$. Development of a numerical method with uniform precision for the entire range $1 \leq \gamma \leq 2$ and the confirmation that as $\gamma \longrightarrow 2^-$, the

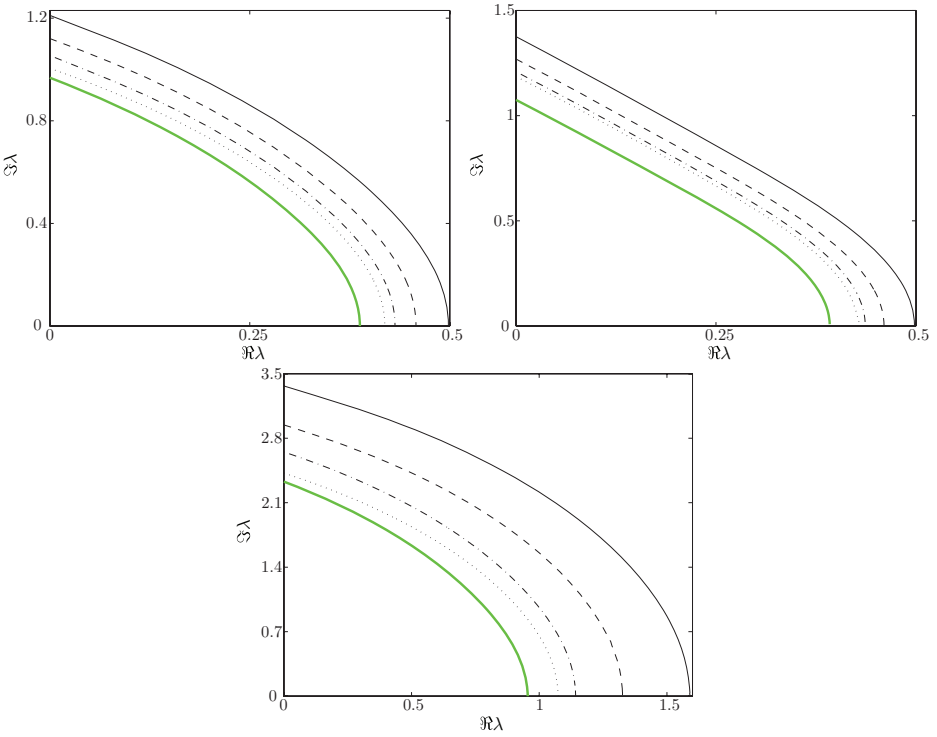

Figure 7. Eigenvalue path parametrized by τ_o for a single spike with the set of exponents $(p, q, m, s) = (2, 1, 2, 0)$ (left), $(p, q, m, s) = (2, 1, 3, 0)$ (right) and $(p, q, m, s) = (3, 2, 2, 0)$ (bottom), and the anomaly exponents $\gamma = 1.05$ (solid), $\gamma = 1.25$ (dashed), $\gamma = 1.5$ (dash-dotted) and $\gamma = 1.75$ (dotted) compared to regular diffusion ($\gamma = 2$, thick green/gray curves, courtesy of M. J. Ward). $D = \mu = 1$.

eigenvalue paths approach the normal curve and the Hopf bifurcation thresholds tend to the normal values, is a topic of a future work. The figures below summarize the effects of Lévy flights within the limitations of the current method for three sets of kinetic exponents. The relevant normal values are brought in Table 1.

Figure 6 shows the eigenfunction $\tilde{A}$ for several values of γ. The tail decay is obviously slower as compared to $\gamma = 2$, however the maxima are higher. Within the range $1 < \gamma \leq 1.75$ the maxima approach the maximum at $\gamma = 2$ monotonously.

Figure 7 depicts the effect of Lévy flights on the location of the eigenvalues (the one with $\Im\lambda > 0$ is shown out of the conjugate pair). It is seen that the Hopf bifurcation frequency is higher, and the modulus of the eigenvalue and in particular the double real eigenvalue are larger than normal. The effect is more pronounced for higher values of p, where the homoclinics are more localized.

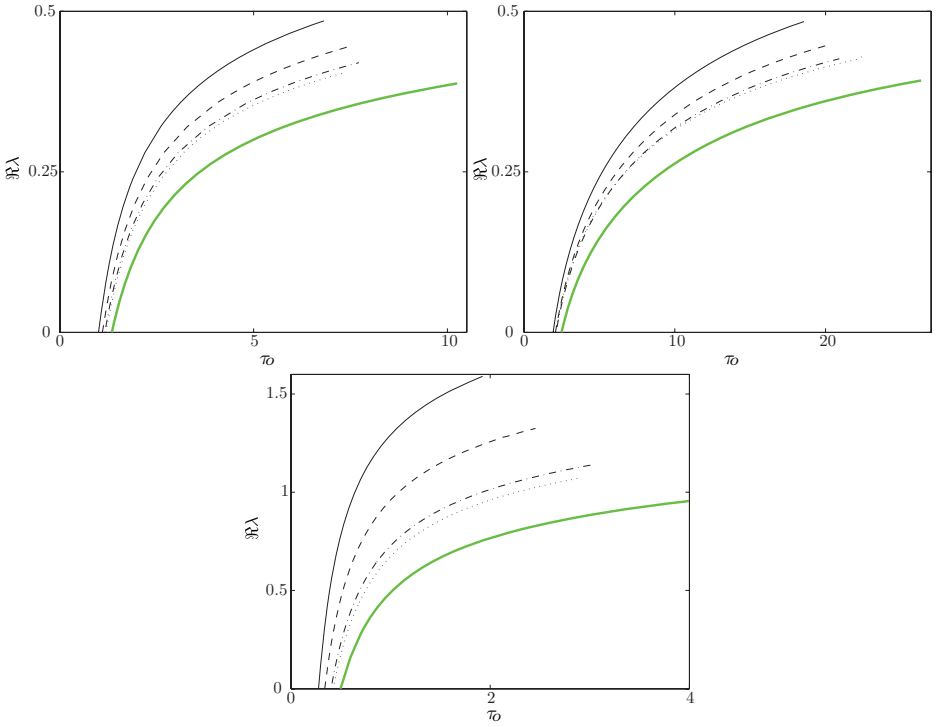

Figure 8. Growth rate $\Re\lambda$ versus τ_o for a single spike with the set of exponents $(p, q, m, s) = (2, 1, 2, 0)$ (left),$(p, q, m, s) = (2, 1, 3, 0)$ (right) and $(p, q, m, s) = (3, 2, 2, 0)$ (bottom), and the anomaly exponents $\gamma = 1.05$ (solid), $\gamma = 1.25$ (dashed), $\gamma = 1.5$ (dash-dotted) and $\gamma = 1.75$ (dotted) compared to regular diffusion ($\gamma = 2$, thick green/gray curves, courtesy of M. J. Ward). $D = \mu = 1$.

Within the range $1 < \gamma \leq 1.75$ the curves $\Im\lambda(\Re\lambda; \gamma)$ approach the normal curve $\Im\lambda(\Re\lambda; 2)$ monotonously. The explicit dependence of the growth rate $\Re\lambda$ on τ_o is plotted in Figure 8. For a fixed value of τ_o the growth rate grows monotonously as γ decreases within the range $1 < \gamma \leq 1.75$.

Figure 9 shows the dependence of the Hopf bifurcation frequency on γ. Figure 10 shows the corresponding value of τ_o. Note that this threshold is not identical to τ_{th}, the Hopf bifurcation threshold of the full system (2), obtained with the numerical scheme used for the homoclinics. However, the general trend of destabilization as γ becomes more anomalous is consistent. In addition, though the parametrization $\Re\lambda(\tau_o)$ and $\Im\lambda(\tau_o)$ in the complex plane is monotonously ascending in τ_o for a fixed value of γ, the dependence of the Hopf frequency and the corresponding value of τ_o on γ is not necessarily monotonous. If an extremum in $\Im\lambda|_{\Re\lambda=0}(\gamma)$ and $\tau_o|_{\Re\lambda=0}(\gamma)$ is obtained, its location is very close for all tested values of D. Also note a peculiar phenomenon of reversal of the dependence $\Im\lambda|_{\Re\lambda=0}(\gamma; D)$: for the sets of

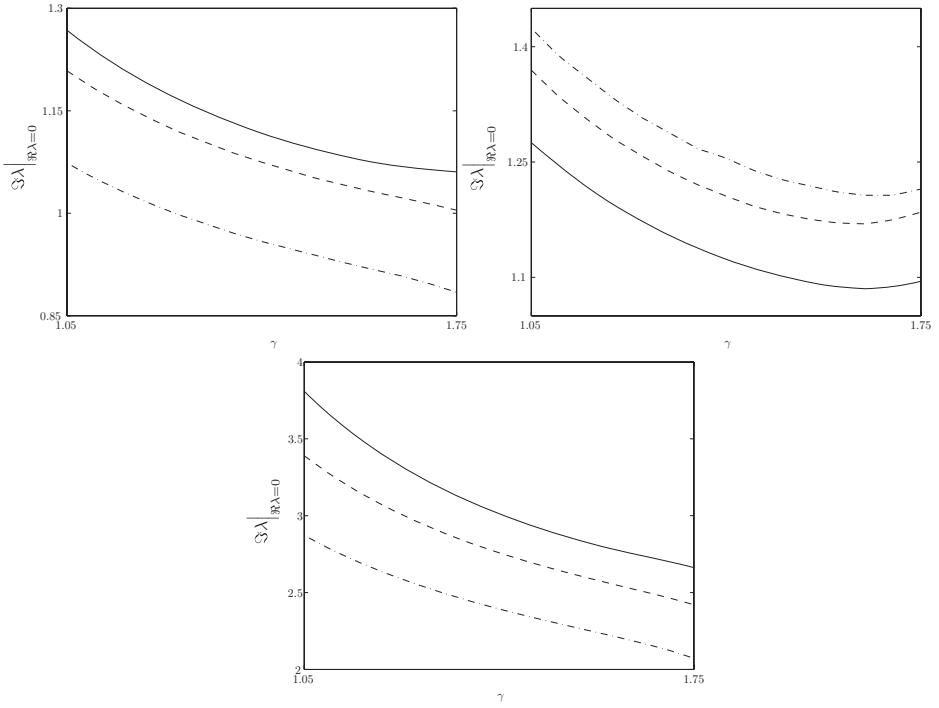

Figure 9. Hopf bifurcation frequency $\Im\lambda|_{\Re\lambda=0}$ versus γ for a single spike with the set of exponents $(p, q, m, s) = (2, 1, 2, 0)$ (left), $(p, q, m, s) = (2, 1, 3, 0)$ (right) and $(p, q, m, s) = (3, 2, 2, 0)$ (bottom), and diffusion coefficients $D = 0.5$ (solid), $D = 1$ (dashed) and $D = 1.5$ (dash-dotted).

exponents (2,1,2,0) and (3,2,2,0) the Hopf frequency decreases with D, whereas for the set (2,1,3,0) the opposite is true, similarly to the results in Table 1. As evident from Table 1, the corresponding curves of τ_o should possess an inflexion point to approach properly the expected values at $\gamma = 2$. This result emphasizes that the dependence of both the Hopf bifurcation frequency $\Im\lambda|_{\Re\lambda=0}(\gamma)$ and the value $\tau_o|_{\Re\lambda=0}(\gamma)$ is more complicated in the range $1.75 < \gamma \leq 2$.

5. Discussion

The Gierer–Meinhardt model was modified to allow the activator to perform a random walk of the type Lévy flight. This feature brings the formal ratio of diffusivities required to sustain patterns closer to realistic, and the effective ratio of the mean square displacement is in favor of the activator for a finite value of ϵ. At the limit $\epsilon \longrightarrow 0$ the effective ratio is undefined, but the existence of patterns implies it is finite. Overall this model is expected to correspond to a realistic diffusivities ratio of the two species.

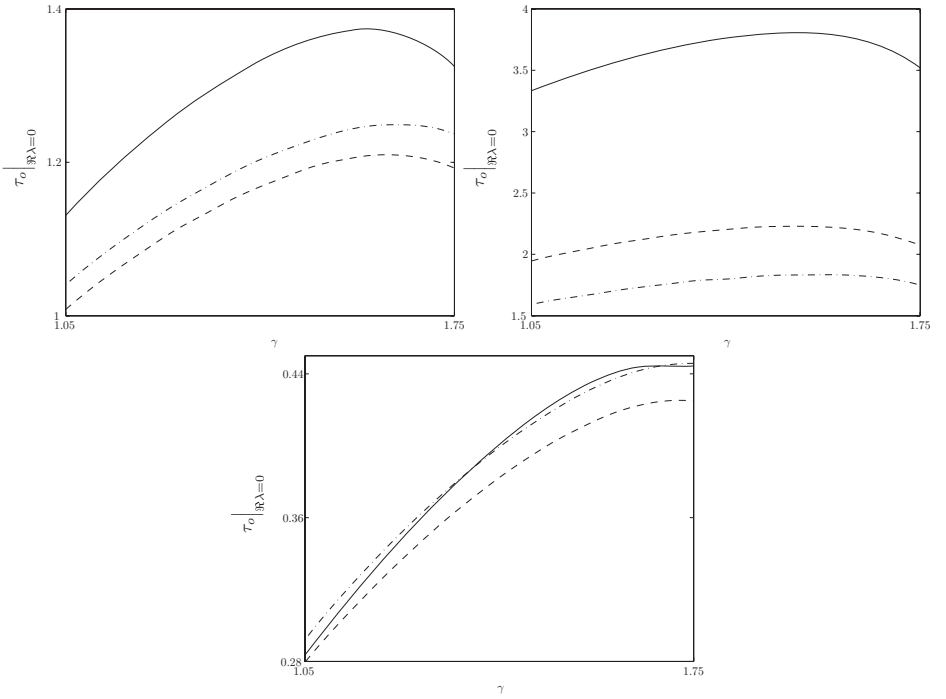

Figure 10. Hopf bifurcation value of $\tau_o|_{\Re\lambda=0}$ versus γ for a single spike with the set of exponents $(p, q, m, s) = (2, 1, 2, 0)$ (left), $(p, q, m, s) = (2, 1, 3, 0)$ (right) and $(p, q, m, s) = (3, 2, 2, 0)$ (bottom), and diffusion coefficients $D = 0.5$ (solid), $D = 1$ (dashed) and $D = 1.5$ (dash-dotted).

The quasi-equilibrium pattern was found to consist of spikes, whose shape is described by a solution to a fractional integro-differential equation. A notable anomalous effect is the algebraic asymptotics of the homoclinic tail versus the regular exponential decay. The equations governing the slow drift of spikes near the equilibrium formation were shown to be of the normal form, but involved a new homoclinic.

The homoclinics were obtained numerically through an auxiliary system of PDEs. The numerical scheme was also used to compute the Hopf bifurcation threshold τ_{th} of the full system and it was found to diminish as γ became more anomalous. A phenomenon of a beating oscillation was discovered near $\gamma \approx 1.2$.

A new type of a nonlocal eigenvalue problem was formulated for eigenvalues of order $\mathcal{O}(1)$. Except for the nonlocality inflicted by the nonlocalized inhibitor species, the differential operator in that problem is also nonlocal, yielding a much more complicated integro-differential equation. The latter was solved numerically and some effects of Lévy flights were examined.

The path followed by the eigenvalues in the right half plane $\Re\lambda(\tau_o; \gamma, D)$ and $\Im\lambda(\tau_o; \gamma, D)$ was found to be sensitive to the presence of Lévy flights, and more so for higher values of p. Related entities manifesting sensitivity to the changes in γ are Hopf bifurcation frequency $\Im\lambda|_{\Re\lambda=0}$ and the corresponding value $\tau_o|_{\Re\lambda=0}$. In all parts of the parameter space tested the anomalous system is less stable in the sense that a broader range of τ_o gives rise to an oscillatory instability. It is also less stable in the sense that the real part of an eigenvalue for a given value of τ_o appears to grow monotonously as γ diminishes.

Most effects of Lévy flights on a single spike appear to be quantitative, and all mentioned curves keep their normal form for a fixed value of γ, even though the dependence on γ might not be monotonous, especially in the range of γ close to the normal value $\gamma = 2$. The finding of no profound changes of the behavior for a fixed value of γ supports the expectation to have the effective ratio of the mean square displacement of the two species as usually in favor of the inhibitor at the limit $\epsilon \longrightarrow 0$, however very close to the realistic ratio of $\mathcal{O}(1)$. To paraphrase, the proposed model allows for pattern formation with formally more desirable and effectively very close to realistic diffusivities ratios, whilst keeping all the known properties of the normal counterpart model.

Acknowledgment

The author kindly thanks M. J. Ward for advice and helpful discussions.

Appendix: Discretization Scheme and Implementation for the Eigenvalue Problem

The equation

$$\mathfrak{D}^{\gamma}_{|y|}\tilde{A} - (1 + \lambda - pu^{p-1})\tilde{A} = u^p, \qquad \lim_{|y|\longrightarrow\infty} \tilde{A}(y) = 0$$

is linear, however the integro-differential operator $\mathfrak{D}^{\gamma}_{|y|}$ involves Cauchy principal value integrals and is nontrivial to discretize. For any $1 \leq \gamma < 2$

$$2\Gamma(-\gamma)\cos\widetilde{\gamma}\,\mathfrak{D}^{\gamma}_{|y|}\tilde{A} = \int_{-\infty}^{y} \frac{\tilde{A}(y) - \tilde{A}(\zeta)}{(y-\zeta)^{\gamma+1}}\,d\zeta + \int_{y}^{\infty} \frac{\tilde{A}(y) - \tilde{A}(\zeta)}{(\zeta-y)^{\gamma+1}}\,d\zeta,$$

and for $\gamma = 1$ the prefactor $2\Gamma(-\gamma)\cos\widetilde{\gamma} = -\pi$ by Lôpital's rule. The infinite domain is approximated by $-y_\infty \leq y \leq y_\infty$ with y_∞ being a finite number sufficiently large to capture properly the algebraically decaying tail. Then the domain $[-y_\infty, y_\infty]$ is divided into $N + 1$ grid points

$$y_i = -y_\infty + \delta y\, i, \quad \delta y = \frac{2y_\infty}{N}, \quad i = 0, \ldots, N.$$

Using the trapezoidal rule for the principal value integrals with integration domains $[-y_\infty, y_{i-1}]$ and $[y_{i+1}, y_\infty]$ for any inner point, and the simplifying with $y_k - y_i = \delta y(k-i)$ yields a linear system of $N-1$ equations

$$\tilde{A}_i \left\{ 1 + \frac{1}{2}\left(\frac{1}{i^{\gamma+1}} + \frac{1}{(N-i)^{\gamma+1}} \right) + \sum_{\substack{k=1 \\ k \neq i-1, i, i+1}}^{N-1} \frac{1}{|i-k|^{\gamma+1}} \right\} - \frac{1}{2}(\tilde{A}_{i-1} + \tilde{A}_{i+1})$$

$$- \sum_{\substack{k=1 \\ k \neq i-1, i, i+1}}^{N-1} \frac{\tilde{A}_k}{|i-k|^{\gamma+1}} = 2(\delta y)^\gamma \Gamma(-\gamma) \cos\widetilde{\gamma} \left(\left(1 + \lambda - p u_i^{p-1}\right) \tilde{A}_i + u_i^p \right),$$

$$\tilde{A}_i = \tilde{A}(y_i), \quad u_i = u(y_i), \quad i = 1, \ldots, N-1$$

equivalent to

$$\mathcal{A}\mathbf{y} = \mathbf{r},$$

where the vectors $\mathbf{y}, \mathbf{r} \in \mathbb{R}^{\mathbf{N-1}}$ with the i-th entries given by $(\mathbf{y})_i = y_i$ and $(\mathbf{r})_i = 2(\delta y)^\gamma \Gamma(-\gamma) \cos\widetilde{\gamma} u_i^p$. The values $A(y_0)$, $A(y_N)$ can be prescribed in two additional equations for the boundary conditions. The simplest choice is $A(y_0) = A(y_N) = 0$. A more sophisticated approach is to use the asymptotics for the algebraic decay the way it was done for the homoclinic computation. In practice the matrix $\mathcal{A}$ is very large and the solution for $\mathbf{y}$ is time consuming. It is possible to estimate the expected decay of $\tilde{A}$ and invert only the core block of the matrix, i.e. a smaller matrix that corresponds to $i = i_*, \ldots, N - i_*$. Then the precise implemenation of the boundary conditions becomes immaterial. Note that the matrix must be assembled in its full size before the inner block is extracted because the assembly of only the inner core block results in an extremely poor precision, as the integrands in the principal value integrals decay quite slowly. Obviously, all parts of the linear system but the addition of λ can be computed only once for a given γ.

In the second part of the numerical procedure the transcedental equation

$$\frac{\chi}{b_m} \int_{-\infty}^{\infty} u^{m-1} \tilde{A}\, dy = 1$$

must be solved. For this purpose the functions u^m and $u^{m-1}\tilde{A}$ must be integrated. To enhance the precision of these integrals the asymptotics of the tails

$$u \approx u(y_*) \left(\frac{y}{y_*} \right)^{-(\gamma+1)}, \quad \tilde{A} \approx \tilde{A}(y_*) \left(\frac{y}{y_*} \right)^{-(\gamma+1)}, \quad y \geq y_*$$

were used with $y_* = y(i_*)$ and $\tilde{A}(y_*)$ being the last available value from the solution of the linear system. Thus

$$b_m = \int_{-\infty}^{\infty} u^m dy \approx 2\int_0^{y_*} u^m dy + \frac{2u_*^m y_*}{m(\gamma+1)-1}, \quad u_* = u(y_*),$$

$$\int_{-\infty}^{\infty} u^{m-1}\tilde{A}\, dy \approx 2\int_0^{y_*} u^{m-1}\tilde{A}\, dy + \frac{2u_*^{m-1}\tilde{A}_* y_*}{m(\gamma+1)-1}, \quad \tilde{A}_* = \tilde{A}(y_*).$$

References

1. R. Metzler and J. Klafter, The random walk's guide to anomalous diffusion: a fractional dynamics approach, *Phys. Rep.* 339:1–77 (2000).
2. T. H. Solomon, E. R. Weeks, and H. L. Swinney, Lévy flights in a two-dimensional rotating flow, *Phys. Rev. Lett.* 71:3975–3978 (1993).
3. T. H. Solomon, E. R. Weeks, and H. L. Swinney, Chaotic advection in a two-dimensional flow: Lévy flights and anomalous diffusion, *Physica D* 76:70–84 (1993).
4. A. Ott, J. P. Bouchaud, D. Langevin, and W. Urbach, Anomalous diffusion in "living polymers": a genuine Lévy flight? *Phys. Rev. Lett.* 65:2201–2204 (1990).
5. M. Boguñ a and A. Corral, Long-tailed trapping times and Lévy flights in a self-organized critical granular system, *Phys. Rev. Lett*. 78:4950–4953 (1997).
6. G. M. Viswanathan, E. P. Raposo, and M. G. E. Da Luz, Lévy flights and superdiffusion in the context of biological encounters and random searches, *Physics of Life Rev.* 5:133–150 (2008).
7. K. B. Oldham and J. Spanier, *The fractional calculus*, Academic Press, New York, 1974.
8. I. Podlubny, *Fractional differential equations*, Academic Press, San Diego, 1999.
9. V. A. Volpert, Y. Nec, and A. A. Nepomnyashchy, Fronts in anomalous diffusion—reaction systems, to appear in Trans. Royal Soc. A.
10. V. A. Volpert, Y. Nec, and A. A. Nepomnyashchy, Exact solutions in front propagation problems with superdiffusion, *Physica D* 239:134–144 (2010).
11. R. L. Frank and E. Lenzmann, Uniqueness and nondegeneracy of ground states for $(-\Delta)^s Q + Q - Q^{\alpha+1} = 0$ in $\mathbb{R}$, arXiv 1009.4042v1.
12. D. Iron, M. J. Ward, and J. Wei, The stability of spike solutions to the one-dimensional Gierer-Meinhardt model, *Physica D* 150:25–62 (2001).
13. M. J. Ward and J. Wei, Hopf bifurcations and oscillatory instabilities of spike solutions for the one-dimensional Gierer-Meinhardt model, *J. Nonlinear Sci*. 13:209–264 (2003).
14. D. Iron and M. J. Ward, The dynamics of multi-spike solutions to the one dimensional Gierer-Meinhardt model, *SIAM J. Appl. Math*. 62:1924–1951 (2002).
15. Y. Nec and M. J. Ward, Dynamics and stability of spike-type solutions to a one dimensional Gierer-Meinhardt model with sub-diffusion, *Physica D.* 241:947–963 (2012).
16. M. J. Ward and J. Wei. Hopf bifurcation of spike solutions for the shadow Gierer-Meinhardt model, *Eur. J. Appl. Math*. 14:677–711 (2003).

University of British Columbia

(Received March 15, 2012)